Experimental Quantification of Critical Parameters for Prediction of Surface Crack Formation in Continuous Casting

Roman Krobath* and Christian Bernhard

One possibility for the off-line training of quality prediction modules in continuous casting is the performance of experiments with samples simulating conditions close to the process. An important point is the surface quality. In the last decade, a new testing setup has been developed called the in situ material characterization by bending (IMC-B) test. This test represents an experimental method, combining solidification, cooling, and deformation in one sequence. It allows the prediction of surface crack formation with respect to the testing conditions. Varying testing parameters enable the determination of the impact of different factors that lead to crack formation during deformation of a casted sample in a hot bending test. The output comprises quantification parameters for damage evaluation, by defining a critical strain for crack formation. Herein, the crack sensitivity for a low carbon construction steel at the bending temperatures of 700–1100 °C is determined. The most critical temperature range is found to be 850–1000 °C.

1. Introduction

The automation techniques in continuous casting are already well advanced. Highly sophisticated process control elements, such as dynamic secondary cooling systems, are already implemented in modern continuous casting machines. Automation is still at a higher level nowadays, because the newest innovations are whole virtual copies of the casting machine, called a digital twin.

These digital twins are constructs of dynamic and complex unions of specific calculation and monitoring modules.[1] Besides the process stability, a main focus lies on the prediction of the product quality. Such quality prediction modules need to be fed with information, which permits a forecast of the chance of problems under the respectively predominating casting conditions. On the one hand, the strand calculation models are provided with accurate material databases to ensure plausible

solidification and temperature calculations of the strand. On the other hand, the impact of loads on the material during casting has to be considered. A system can learn from the inspection of the products for defects in further process steps. This has the advantage of a self-learning process, but bears the risk of disregarded influencing factors and misinterpretation of results. A second method is to create data from experimental investigations with respect to the process and feed it to the calculation models. A requirement for the plausibility of the information generated is an experimental simulation under near-process conditions. Exaggerated and with respect to selected topics, such experiments can be called "experimental twins." A central aspect of quality prediction is the surface crack formation. The process factors and parameters that influence the formation and finally lead to surface cracks are widely spread. This results in several possible types of surface cracks and defects, which are summarized in earlier publications.[2–4] An "experimental twin" for the mechanical triggering of certain surface cracks in the material should cover process parameters as well as material behavior close to process conditions.

In the past decades—back to the 1960s—the strand shell ductility was characterized mostly by conventional hot ductility testing. In general, the experiments were performed as uniaxial hot tensile tests.[5] Compression and torsion tests were less common. Varying deformation temperatures with respect to the deformation parameters, the heat treatment and the steel composition allow the comparison of the results in ductility curves, which show the reduction of area (RA) values depending on the deformation temperatures. Adjusted testing sequences were carried out to simulate near-process conditions, e.g., coarse grain annealing and fluctuating cooling sequences. Results are summarized in extensive collections of works and publications.[5–10] There are methods where the sample is particularly melted in the gauge length, e.g., see the studies given by Revaux et al.[11,12] The initial melted and solidified tests generally show less RA. To use results of ductility curves for the prediction of surface crack formation, critical RA values are defined. Schwerdtfeger and Spitzer[13] developed an approach regarding how RA values can be even better quantified for surface cracking criteria, converting them to a critical cracking strain. These findings are highly sophisticated; however, the high strains to fracture in the tensile experiments and the possible resulting

Dr. R. Krobath, Prof. C. Bernhard
Ferrous Metallurgy
Montanuniversitaet Leoben
Franz-Josef-Strasse 18, 8700 Leoben, Austria
E-mail: roman.krobath@unileoben.ac.at

The ORCID identification number(s) for the author(s) of this article can be found under https://doi.org/10.1002/srin.202000234.

recrystallization and deformation-induced phenomena in the sample material at specific temperatures are sometimes factors of uncertainty. This results when the simulation of the surface crack formation in continuous casting is considered, which occurs at very low tensile strain, and is why Crowther[14] came to the conclusion that a hot bending test would be a more suitable method for the simulation of surface crack formation closer to continuous casting conditions. Such experiments were already developed half a century ago. Schmidt and Gross[15] investigated influencing factors on network crack formation with reheated samples in a bending test in the 1960s. Some years later, Lankford[16] published a bending testing method where the samples got reheated to a temperature above 1400 °C before they got cooled and deformed in a temperature range of 930–1260 °C. The induced strains exceeded 24%. Burden et al.[17] also worked with reheated samples in a bending test using heavy deformation. To improve the approach to process conditions, Yasumoto et al.[18] worked with in situ casted samples that got deformed in a three-point bending test. The strain was in the single-digit range, and the cracks got evaluated macroscopically. Crowther et al.[19] developed an experiment including in situ casted samples, as well. The results of the different microalloyed steel grades regarding surface cracking were significant. The test aimed to simulate cracking behavior in thin slab casting. Another bending method for investigating the susceptibility to surface crack formation was developed at Montanuniversitaet Leoben, called the in situ material characterization by bending (IMC-B) test. The earlier development of the test is described in detail in the work of Krajewski.[20] The method has been further advanced, as shown in publications by Krobath et al.[21–23] Nowadays, it represents an experimental method combining solidification, controlled cooling, and defined deformation of samples in one testing sequence. The next chapters explain the state of the art of the experiment and present the analyses of the samples in addition to selected results.
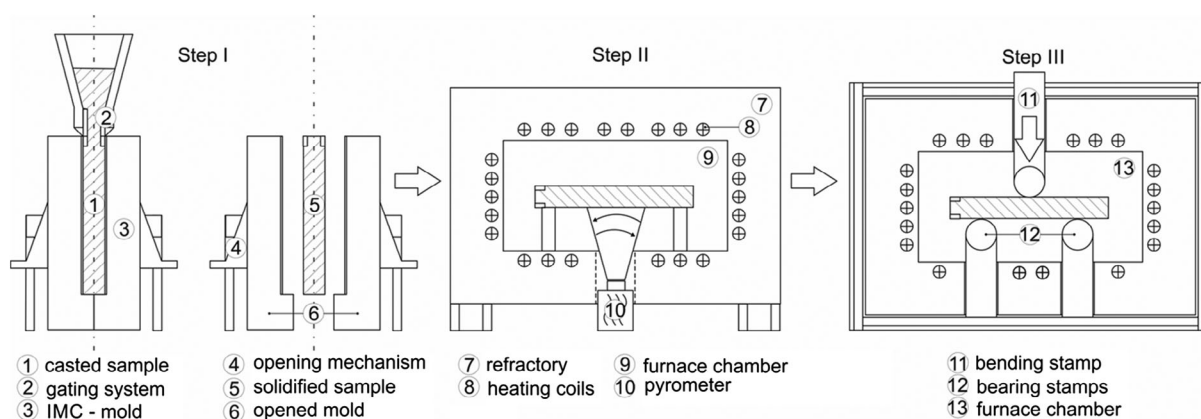
2. Experimental Section

2.1. Description of Methods

In the IMC-B test, every sample is casted separately in a steel mold where solidification and mold cooling take place.
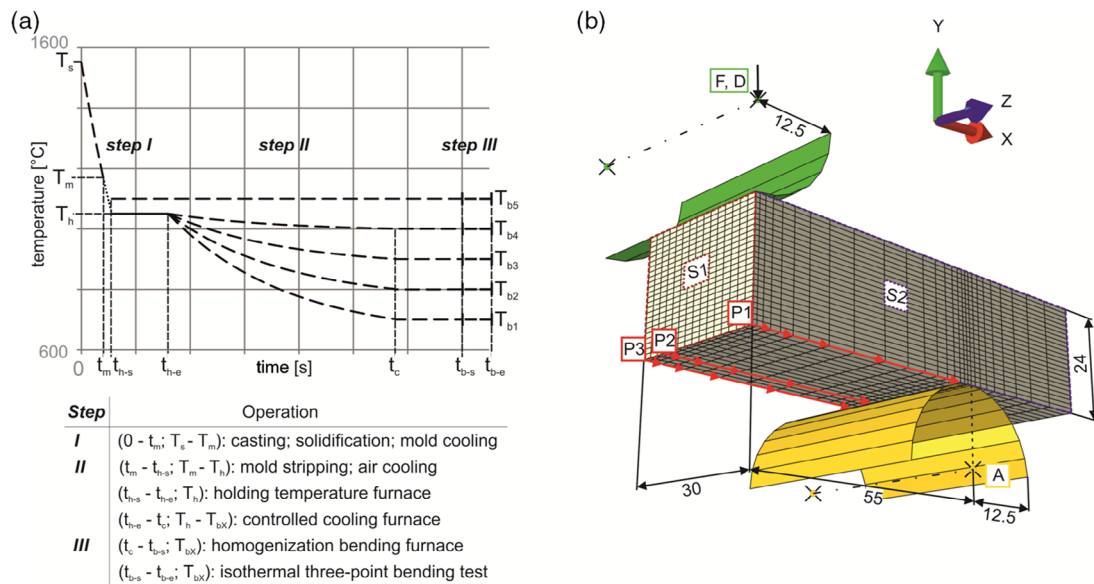
The residual time in the mold is adjusted to the aim of the simulated process conditions. **Figure 1** shows the whole workflow. The split construction of the mold allows a fast and easy removal of the sample finishing step I of the test. Continuing in step II, the sample is cooled down according to a specific thermal sequence reaching a certain target value, which represents the later on bending temperature. This is managed by a stepwise apposition of chamber furnaces with varying temperatures. During this thermal cycle, the sample surface temperature is continuously measured with an optical pyrometer.

For bending, the sample is positioned in bending equipment on the bearing stamps, where the temperature field is homogenized at bending temperature for times between 30 and 120 s. At a defined starting point, isothermal bending of the sample takes place, realized with the movement of the bending stamp. The well-controllable facility allows accurate bending parameters, either force or displacement controlled. This deformation of the sample should simulate local strand shell deformation, e.g., during bending and straightening. Finally, the sample is cooled to room temperature by smooth cooling to minimize the thermal and transition-induced stresses and strains, or it is quenched to freeze the microstructure. Every sample is descaled, and the surface is investigated in detail with a digital microscope. The defects and cracks are documented with respect to their position on the sample surface.

Figure 2a shows the schematic temperature–time curves for the IMC-B test. The sequence is defined by significant points within the three main steps. When displacement controlled tests are performed, the deformation characteristics are given by stamp velocity and displacement. The velocity is constant during the loading and unloading stages. The material behavior during bending is simulated with the finite-element (FE) software package Abaqus. The material model is especially adjusted to the material behavior of the directly casted samples, which can be significantly different from reheated samples. The constitutive material model combines elastic, plastic, and viscoplastic effects, allows accurate analyses of the stress and strain fields in the sample, and is explained by Krobath et al. in a recently published work.[24] Figure 2b shows a draft of the FE model with the mesh and the significant control and evaluation points. To save calculating time, a quarter of the sample with symmetry planes in the x- and z-directions is used ("S1, S2"). All dimensions are given in

Figure 1. Workflow of the IMC-B test.

① casted sample ④ opening mechanism ⑦ refractory ⑨ furnace chamber ⑪ bending stamp
② gating system ⑤ solidified sample ⑧ heating coils ⑩ pyrometer ⑫ bearing stamps
③ IMC - mold ⑥ opened mold ⑬ furnace chamber

Figure 2. a) Schematic cooling curves within marked significant points including definition. b) FE model for simulating material behavior in the three-point bending test.

millimeters. The translational and rotational values of the bearing are fixed (point "A"). Evaluation of the force and displacement takes place at the control point "F, D." The evaluation of stresses and strains on the sample surface with respect to the distance of the bending axis takes place following the three paths "P1, P2, and P3." P3 represents the sample corner, whereas P1 represents the center line of the surface. The 2D evaluations in the x-direction mean the average values of the three paths.

A main characteristic of the IMC-B test is the usage of in situ cast samples. The coatings enable controlled heat flux in the mold resulting in directional dendrite growth and associated coarsening of the dendrite and columnar grain structure, as shown in **Figure 3**b. Due to the well-controlled heat withdrawal, the resulting structure is similar to the structure of a strand shell surface;

see Presslinger et al.[26] and Figure 3a. Metallographic investigations reveal the coarse columnar austenitic grain structure of IMC-B samples, shown in Figure 3d for a 0.17 wt% C steel. The mean grain size depends mainly on the heat withdrawal in the mold and can, therefore, also be adjusted to the grain size at the slab surface, as shown by Reiter et al.[27] It should be mentioned that the steel composition also plays an important role for the appearance of the austenite grain structure in directional solidification. Ohno et al.[25] show these correlations with samples investigated with rapid directional solidification equipment. A typical coarse columnar austenite grain structure for plain carbon steels in the range of 0.1–0.2 wt% C is shown in Figure 3c.

IMC-B tests may be performed either after controlled cooling in air or protection by inert gas, such as Ar. Normally, the
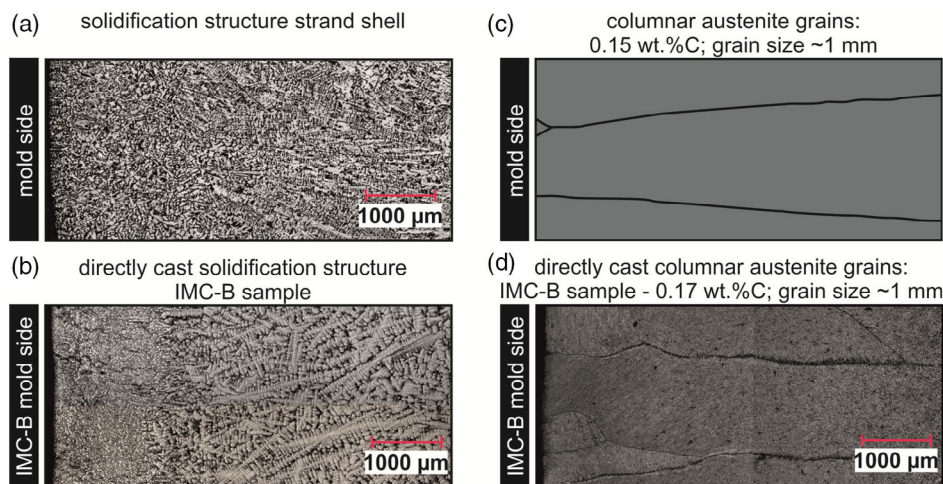
Figure 3. Comparison of microstructures: a) Solidification structure strand shell, b) solidification structure IMC-B sample, c) coarse columnar austenite grains (redrawn scheme),[25] and d) typical coarse columnar austenite grains in IMC-B sample—0.17 wt% C steel.

bending tests are performed after cooling in air. This results in a strong oxidation of the surface but also, depending on the steel composition and here, namely, the content of certain elements, such as Si, Al, and Mn, in intergranular (IG) and inner oxidation. A recent study of Krobath et al.[23] shows the harmful impact of a certain stronger IG oxidation on the formation of surface cracks in the bending experiments. It points at a possible strong influence of oxidation reactions of the sample surface with respect to tested conditions and composition and makes the results of the bending experiment dependent on the cooling conditions. If this effect should be suppressed, the sample may also be shielded by inert gases during cooling, and surface oxidation is mostly prevented.

Beside the conditions during solidification and cooling, a main focus lays on the sample steel composition. The melting and alloying procedure enables nearly free adjustment of the steel composition, realized by the usage of high purity iron as base material and stepwise adding of high purity alloying elements. Therefore, it is possible to produce samples of steels with very low alloying contents e.g., ultralow carbon steels, but also of high alloyed steel grades with extraordinary alloying concepts. The possibility of changing the content of individual elements is an important advantage of the IMC-B testing method, because small differences can already have a significant effect on the material behavior during the bending test and, furthermore, on the results regarding crack formation.

In summary, the whole set of testing parameters for the conventional IMC-B test includes: 1) steel composition with specific element contents; 2) temperature sequence, e.g., according to Figure 2a within cooling conditions after the bending test; 3) atmosphere during cooling and bending; and 4) bending parameters.

2.2. Testing Parameters

The basic composition for the following results is listed in **Table 1**. It represents an Al deoxidized 0.17 wt% C construction steel. The significant points for the temperature sequence are shown in **Table 2**. The liquid steel is poured in the mold with a starting temperature of $\approx 1550\,°C$. The time of 45 s in the mold results in a surface temperature of $\approx 1180\,°C$ afterward. The holding temperature T_h is $1050\,°C$ (except for samples with a bending temperature T_b of $1100\,°C$), and the total time at the start of bending is 700 s. It is related to the start of the straightening process of a slab caster with a casting speed of $1.2\ m\ min^{-1}$ and a slab thickness of 225 mm; see Krajewski et al.[28] The bending temperature ranges between 700 and $1100\,°C$ in

Table 1. Basic steel composition—all values in wt%.

C	Si	Mn	P	S	Al	N
0.17	0.4	1.55	0.01	<0.004	0.03	<0.008

Table 2. Significant points in the temperature sequence.

t_m [s]	T_m [°C]	T_h [°C]	t_{h-e} [s]	t_{b-s} [s]	T_{bX} [°C]
45	≈ 1180	1050	160	700	700–1100

$50\,°C$ steps. The testing sequence is done at air atmosphere. After the bending test, each sample is cooled to room temperature with mild cooling rates between ≈ 5 and $\approx 1\,°C\ min^{-1}$, depending on the value of T_b.
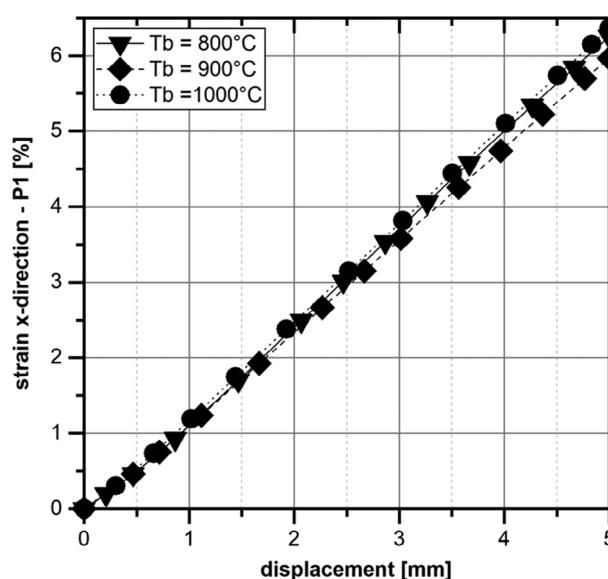
The bending stamp velocity for the loading and unloading step is $0.04\ mm\ s^{-1}$. Stamp displacements of 3 and 5 mm are applied for the whole temperature range. Tests get reproduced at $T_b = 850\,°C$ and $T_b = 1050\,°C$. Stamp displacements of 2, 3, 4, and 5 mm are tested at the bending temperature of $900\,°C$. For the validity of reproduction, in this case, every test is performed twice.
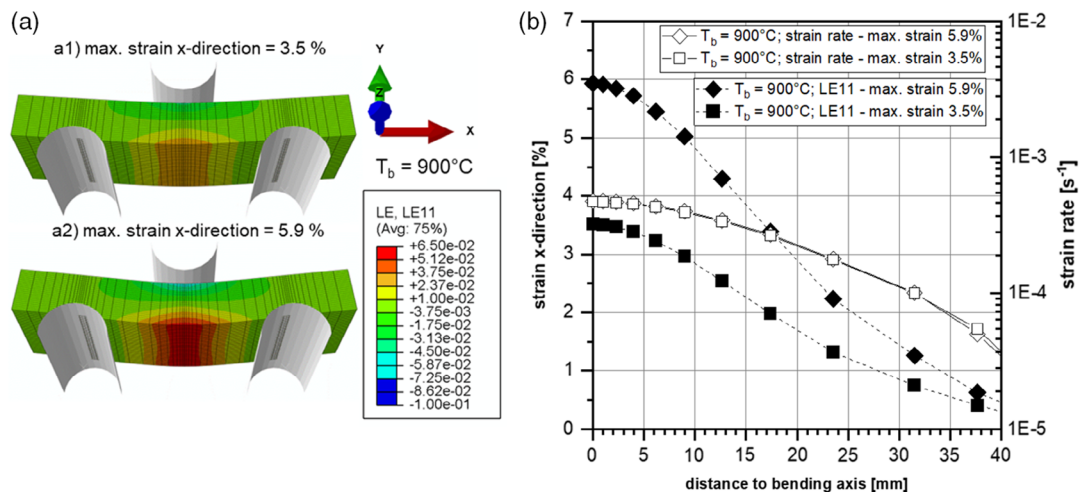
3. Results

3.1. Simulation

The induced maximum strain and the strain distribution on the sample are triggered by the displacement of the stamp. In **Figure 4**, the strains in the x-direction (starting point analyses path P1, Figure 2b) in the bending axis against the stamp displacement at representative bending temperatures of 800, 900, and $1000\,°C$ are shown. The progression is nearly linear for all three temperatures. Conventional IMC-B tests are performed with the maximum displacements up to 5 mm. A total displacement of 5 mm leads to the maximum total strains between 5.9% ($T_b = 900\,°C$) and 6.4% ($T_b = 1000\,°C$) for the investigated temperature range. Differences in the strain distributions are according to changes in the material behavior between the bending temperatures.

An advantage of the three-point bending test is an induced strain distribution on the sample surface. This enables the investigation of the impact of strains from 0 to a maximum strain on the formation of cracks with respect to the distance from the bending axis in a certain range of strain rates. **Figure 5**a shows the total strain distributions in the x-direction (LE11) for two

Figure 4. Total strain in the x-direction in bending axis according to the stamp displacement.

ADVANCED
SCIENCE NEWS
www.advancedsciencenews.com

steel
research
international
www.steel-research.de

Figure 5. a) Strain distributions at $T_b = 900\,°C$: a1) max. strain in bending axis 3.5% and a2) max. strain in bending axis 5.9%. b) Mean strain values in the x-direction and the corresponding strain rates against the distance to the bending axis corresponding to the bending cases in (a).

cases of stamp displacement and resulting maximum strains at $T_b = 900\,°C$, a1) displacement = 3 mm and max. strain = 3.5% and a2) displacement = 5 mm and max. strain = 5.9%. It illustrates that the higher deflection results in a higher maximum strain, but it also covers the strain ranges of the sample with a lower deflection.

The detailed strain evaluations of the two bending cases visualized in Figure 5a are shown in the diagram in Figure 5b. It contains the mean strain values in the x-direction and the corresponding strain rates against the distance to the bending axis. The strain rates coincide nearly fully within the values of 3×10^{-5}–$4.7 \times 10^{-4}\,s^{-1}$. The values correlate with surface strain rates during straightening in continuous casting, which are calculated to be in the range of max. $\approx 4 \times 10^{-4}\,s^{-1}$ to max. $\approx 6 \times 10^{-5}\,s^{-1}$, with respect to machine parameters.[29] In contrast, the gap between the strains gets higher with decreasing distance to the bending axis. At an interval of 40 mm, the strains of both cases are still below 0.5%. The test with a higher deflection reaches 2% surface strain at ≈ 25 mm distance. For the test with lower deflection, it is obtained at 17.5 mm. This strain is known as the guide value for maximum mechanically induced strains during straightening.[3,14] As the value can shift, e.g., due to thermal strains and higher strains in the case of notch effects in oscillation marks or surface pores,[30] the higher strains are also considered for interpretation, because they are still clear in the single-digit range. The diagram expresses the advantage that positions of documented cracks can be directly related to a certain induced strain, which is a fundamental requirement for a meaningful interpretation of results.

3.2. Surface Crack Investigation

The defects have to be carefully investigated, as the morphology can obtain the information of the temperature zone where it formed. Cracks with paths through the bulk of austenite grains and fully dendritic morphology indicate defects formed in the first ductility trough during solidification. The triggers are

remaining liquid phases at the liquid–solid interface, enriched with segregated elements and a lower melting point. Initialized strains are concentrated at these phases, resulting in a formation of pores growing to cracks with increasing strain. The temperature range reaches from solidus to the "zero ductility temperature" of $\approx 50\,°C$ below solidus.[31–33] **Figure 6** shows a scheme of a slab with several possible types of surface cracks. Figure 6d shows the longitudinal cracks, which are usually, originating already in the mold, related to the cracking mechanisms in the first ductility trough.[3,4] The cracks may also grow during secondary cooling and straightening.[3,34] Such kind of cracks can be found in the surface of IMC-B samples, but for the evaluation of the ductility and the susceptibility for crack formation in the area of 700–1100 °C, these defects cannot be considered. Nonetheless, they provide information concerning the behavior during solidification in the mold.

In general, cracks formed due to the bending of the sample are IG at the austenite grain boundaries and range from $\approx 50\,\mu m$ to ≈ 3 mm in length. Figure 6a–c shows different crack arrangements on the surface of IMC-B samples originated in the course of bending and a comparison with possible slab surface issues within the positions. Figure 6a shows the typical singular IG cracks, which are the most frequently observed crack type. They can be found at the broadside and the corner. Figure 6b shows the crack clusters. They present a special type of cracks with a lot of small oriented cracks in which a separation of the singular cracks is already difficult. Such issues often form when a very critical state is simulated in samples with a substantial number of cracks, observed often at microalloyed steel samples. Network cracks, shown in Figure 6c, are unoriented cracks that can form on samples where pre-defects such as IG high-temperature oxidation have taken place.[23]

3.3. Quantification Parameters

The first quantification parameter of the crack formation is the total number of cracks. It indicates the surface damage due to the
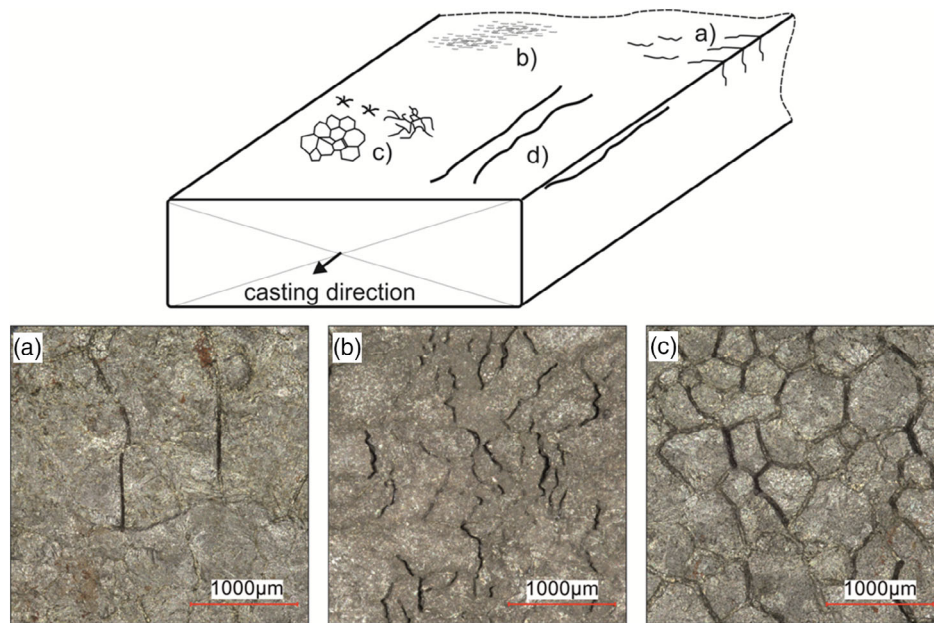
Figure 6. Scheme of a continuous casting slab with surface defects: a) singular oriented IG cracks, b) crack clusters, c) network cracks, and d) longitudinal cracks.

bending test, considering all testing parameters, including the bending case. **Figure 7**a shows the results for the described testing parameters and the two bending cases in Figure 5. The labeled explanation shows the max. strain mean value for the investigated temperature range of 700–1100 °C. At 3.6%, the four bending temperatures between 850 and 1000 °C show a number of cracks between 18 and 28. All other remaining samples revealed no cracks at the sample surface. The test at 850 °C was successfully reproduced with the values of 18 and 22. The temperatures where no cracks formed can be described as not critical, but because of the only small differences in the number of cracks at the other temperatures, no clear statement as to which temperature is the most critical is possible for this deflection.

In comparison, the higher strains lead to significantly higher gaps. The samples in the lower temperature range of 700–750 °C still show no cracks. This already leads to the first conclusion that with the current testing sequence, this steel reveals no susceptibility to surface cracking at these temperatures. The 37 cracks are documented for a bending temperature of 800 °C. The high temperatures of 1050 and 1100 °C show 59 and 11 cracks, respectively. A second sample at 1050 °C with 64 cracks shows a similar result. The most critical temperatures are also found to be between 850 and 1000 °C. But for the higher stains, a considerable deterioration from 113 (1000 °C) to 229 (850 °C) cracks is identified. It has to be mentioned that the scale for the number of cracks is intermittent at 300 and shows a maximum value of 800. According to Krobath et al.,[23] a maximum number of
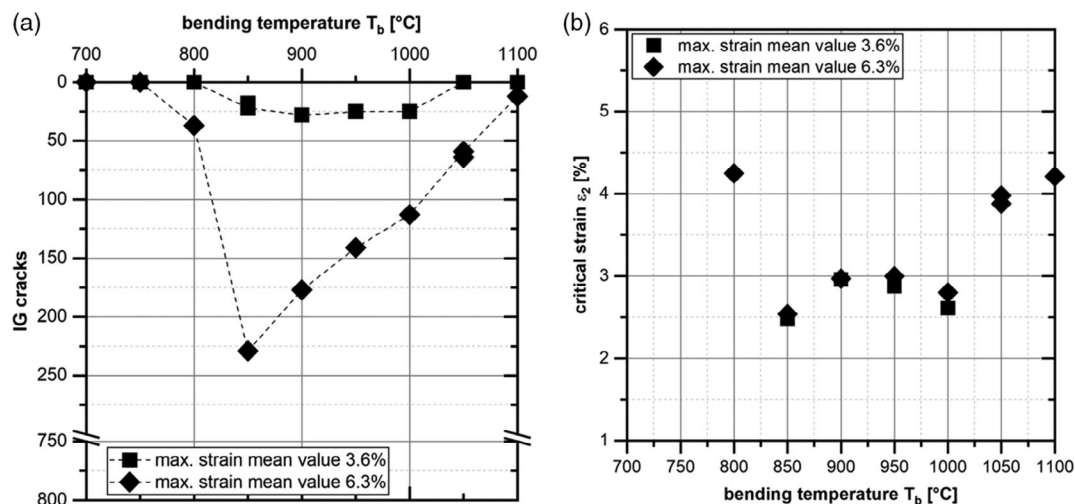
Figure 7. a) Number of IG cracks for the whole temperature range and the two bending cases. b) Corresponding critical strain ε_2 for all samples.

**ADVANCED
SCIENCE NEWS**

www.advancedsciencenews.com

**steel
research**
international

www.steel-research.de

cracks that can be described separately is ≈800. Above this limit, a significant distinction according to the degree of damage regarding the number of cracks becomes impossible.

Within the total number of cracks, noncritical temperatures and temperatures with significantly more cracks can be explained. To reach a quantified appraisal of the crack formation regarding continuous casting, a critical strain for first crack formation is established. According to the crack positions and the development of the strains with respect to the maximum stamp displacement and bending temperature, the strain for first crack formation is determined. As this is an exceptionally meaningful value, the critical strain ε_2 defines the lowest strain value where two cracks have already formed on the sample surface with an accuracy of 0.01%. This ensures the validity of this parameter. The diagram in Figure 7b presents the ε_2 values according to the samples in Figure 7a. The noncritical temperatures of 700 and 750 °C show no cracks, which means the value of ε_2 exceeds 6.3% and is, therefore, not relevant for conventional continuous casting. At 800, 1050, and 1100 °C, the values of ε_2 range between 4.25% (800 °C) and 3.88% (1050 °C). This correlates with the samples with the maximum strains of 3.6%, which show no cracks, as the critical strains exceed the maximum induced strain. The samples with the higher number of cracks at 850–1000 °C also reveal the lowest values of ε_2. At 900 and 950 °C, all four values are nearly superimposable at 3%. At 1000 °C, the lower value reaches 2.61%, and at 850 °C, the most critical behavior, with the ε_2 of 2.49%, is observed. The reproducibility at 850 °C (max. strain 3.6%) and 1050 °C (max. strain 6.3%) is again very accurate.

Figure 8a shows the number of cracks for samples with continuously increasing maximum strain at $T_b = 900$ °C. For the validity of reproduction, every test is performed twice. The two samples with maximum strains below the critical strain limit do not reveal significant cracks on the surface. When that "barrier" is exceeded, the number of cracks grows with a nearly exponential progression. But, the critical strain values in Figure 8b confirm that the first crack formation does not depend greatly on the maximum induced strain. All values of ε_2 are in the range between 2.49% and 3.35%.

4. Discussion

Samples with differing maximum strains show dependency in the maximum strain and the number of cracks, but similarity in the critical strain ε_2. This points at certain strain-induced underlying mechanisms. More precisely, a high amount of deformation-induced AlN precipitates for the highest strains is plausible. Furthermore, these results indicate that for a steel composition with a certain set of testing parameters, the critical strain for first crack formation does not depend on the maximum induced strain. In fact, ε_2 represents a factor that shows the surface ductility of a current state dependent on the whole set of testing parameters. In addition, the highest maximum strain values enable the most detailed grading of results and provide more information of the material. Therefore, it is suggested that this deflection be standard for the experimental simulation cases. Both parameters—the number of cracks and the critical strain—are verifiable, even if the critical strain is more evident regarding surface cracking in continuous casting. Thus, for the best comparability of IMC-B data, a certain IMC-B cracking index should be established that also considers the severity of the defects, e.g., in the case of maximum crack depth.

The results permit an evaluation regarding surface cracking in the second ductility trough. Basically, the critical strains are higher than the mechanically induced strains in a conventional straightener. In the case of the investigated steel grade and testing parameters, the risk of surface cracking is moderate, although the most critical temperature is 850 °C. It should be kept in mind that with additional thermal strain contributions or deep oscillation marks, the total strains on the strand surface can increase. The results are valid for the current testing parameters and steel composition. Changes in the parameters can, however, have a detrimental impact on the surface ductility; for example, less cooling in the mold, which leads to the high temperatures of >1200 °C for a certain time after the mold, can trigger pre-defects on the sample surface and bring about poor ductility in the critical temperature range; see Krobath et al.[23] In the course of such conditions, the critical strain ε_2
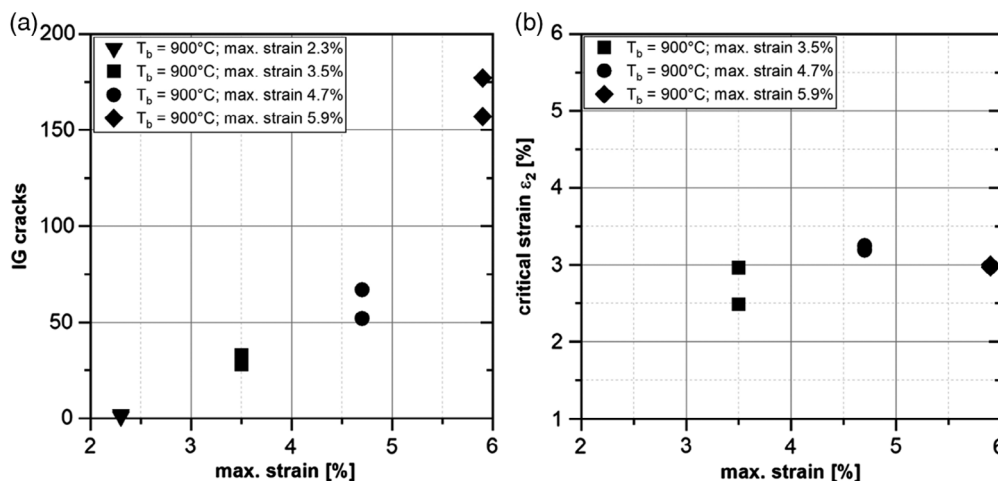
Figure 8. a) Number of IG cracks for continuously rising maximum strains at $T_b = 900$ °C. b) Corresponding critical strain ε_2 at $T_b = 900$ °C.

can drop to 1.7% at a bending temperature of 900 °C for the same steel composition. Therefore, it should be kept in mind that the testing conditions have to be as near as possible to the real casting process, which is simulated, to reach the best goals in optimizing the process. Using the data of the IMC-B results for surface crack prediction models and calculations proves highly beneficial, because a vast number of scenarios can be simulated to gain information for different mechanisms leading to surface cracks.

5. Conclusion

In this study, the determination of the susceptibility to surface cracking in the range of the second ductility trough with the IMC-B test is exemplified. The most important characteristics of the IMC-B test can be summarized as follows: 1) similar microstructure compared with the strand shell—directional dendrite growth and columnar austenite grains; 2) surface phenomena due to contact with atmosphere—no inert atmosphere in conventional IMC-B testing; and 3) spectrum of strains and strain rates on the sample surface—information about the first crack formation.

The results of the evaluation of a 0.17 wt% C steel are expressed with the number of cracks and the critical strain for crack formation. The most important results are as follows: 1) the most critical temperature range is revealed at 850–1000 °C; 2) noncritical behavior is observed at 700–750 °C; and 3) the lowest critical strain value of 2.49% shows the sample with a bending temperature of 850 °C.

Acknowledgements

Conflict of Interest

The authors declare no conflict of interest.

Keywords

[1] R. Leitner, D. Fuchshuber, C. Brugger, P. Pennerstorfer, in *Proc. of the 4th ESTAD*, Steel Institute VDEh, Dusseldorf, Germany **2019**.
[2] J. K. Brimacombe, K. Sorimachi, *Metall. Mater. Trans. B* **1977**, *8*, 489.
[3] E. S. Szekeres, in *Proc. of the 6th Int. Conf. on Clean Steel*, OMBKE, Balatonfured, Hungary **2002**.
[4] G. Xia, K. Burgstaller, C. Fürst, B. Harrer, E. Milosch, A. Samoilov, in *Proc. of the 8th ECCC*, ASMET, Graz, Austria **2014**.
[5] K. Schwerdtfeger, *Crack Susceptibility of Steels in Continuous Casting and Hot Forming*, Verlag Stahleisen GmbH, Dusseldorf, Germany **1994**.
[6] D. N. Crowther, B. Mintz, *Mater. Sci. Tech.* **1986**, *2*, 671.
[7] H. G. Suzuki, PhD Thesis, Tohuku University **1981**.
[8] R. Abushosha, R. Vipond, B. Mintz, *Mater. Sci. Tech.* **1991**, *7*, 1101.
[9] B. Mintz, J. R. Banerjee, *Mater. Sci. Tech.* **2010**, *26*, 547.
[10] B. Mintz, D. N. Crowther, *Int. Mater. Rev.* **2010**, *55*, 168.
[11] T. Revaux, P. Deprez, J. P. Bricout, J. Oudin, *ISIJ Int.* **1994**, *34*, 528.
[12] T. Revaux, J. D. Guerin, J. P. Bricout, *Mater. Sci. Tech.* **2004**, *20*, 19.
[13] K. Schwerdtfeger, K. H. Spitzer, *ISIJ Int.* **2009**, *49*, 512.
[14] D. N. Crowther, in *Proc. of the Vanitec Symp.*, Vanitec, Bejing, China **2001**.
[15] F. Schmidt, O. Gross, *Steel Int.* **1967**, *3*, 11.
[16] W. T. Lankford, *Metall. Trans.* **1972**, *3*, 1331.
[17] M. H. Burden, G. D. Funnel, A. G. Whitaker, J. M. Young, in *Proc. Solidification and Casting of Metals*, London, UK **1979**.
[18] K. Yasumoto, Y. Maehara, T. Nagamichi, H. Tomono, *Tetsu Hagane* **1989**, *73*, 1381.
[19] D. N. Crowther, M. J. W. Green, P. S. Mitchell, *Mater. Sci. Forum* **1998**, *284–286*, 469.
[20] P. Krajewski, PhD Thesis, Montanuniversitaet Leoben, **2013**.
[21] R. Krobath, C. Bernhard, S. Ilie, J. Six, S. Hahn, P. Pennerstorfer, *La Metall. Italiana* **2017**, *2017*, 5.
[22] R. Krobath, C. Bernhard, in *Proc. of the AISTech2017*, Association for Iron & Steel Technology, Nashville, TN, USA **2017**.
[23] R. Krobath, C. Bernhard, S. Ilie, J. Six, S. Hahn, P. Pennerstorfer, *BHM* **2019**, *164*, 461.
[24] M. Krobath, R. Krobath, C. Bernhard, W. Ecker, *Materials* **2020**, *13*, 2281.
[25] M. Ohno, S. Tsuchiya, K. Matsuura, *ISIJ Int.* **2015**, *55*, 2374.
[26] H. Presslinger, M. Mayr, E. Tragl, C. Bernhard, *Steel Res. Int.* **2006**, *77*, 107.
[27] J. Reiter, C. Bernhard, H. Presslinger, *Mater. Charact.* **2008**, *59*, 737.
[28] P. Krajewski, R. Krobath, C. Bernhard, J. Miettinen, S. Louhenkilpi, S. Ilie, T. Schaden, *BHM* **2015**, *160*, 109.
[29] X. Zhang, H. Zhu, W. Huang, B. Shi, A. K. Tieu, *Int. J. Mater. Prod. Tecnol.* **2013**, *47*, 126.
[30] M. Suzuki, H. Hayashi, H. Shibala, E. Toshihiko, L. In-Jae, *Steel Res.* **1999**, *70*, 412.
[31] C. Bernhard, R. Pierer, A. Tubikanec, C. Chimani, in *Proc.of the Continuous Casting and Hot Rolling Conf.*, Linz, Austria **2004**.
[32] S. Ilie, J. Reiter, H. Presslinger, J. Fluch, C. Bernhard, in *Proc. of the 6th ECCC*, AIM, Riccione, Italy **2008**.
[33] R. Pierer, C. Bernhard, C. Chimani, *BHM* **2004**, *149*, 95.
[34] H.-L. You, X.-H. Liu, *J. Cent. South Univ. Technol.* **2010**, *17*, 235.